CHEMISTRY OF MATERIALS

ARTICLE

pubs.acs.org/cm

Layered Li_xMoO_2 Phases with Different Composition for Electrochemical Application: Structural Considerations

D. Mikhailova,*[,†,‡] N. N. Bramnik,[‡] K. G. Bramnik,[‡] P. Reichel,[†] S. Oswald,[†] A. Senyshyn,[‡,§] D. M. Trots,[∥,⊥] and H. Ehrenberg[†,‡]

[†]Institute for Complex Materials, IFW Dresden, Helmholtzstr. 20, D-01069 Dresden, Germany

[‡]Institute for Materials Science, Darmstadt University for Technology, Petersenstr. 23, D-64287 Darmstadt, Germany

[§]Forschungsneutronenquelle Heinz Maier-Leibnitz FRM-II, Technische Universität München, Lichtenbergstr. 1, D-85747 Garching near München, Germany

[∥]Bavarian Research Institute of Experimental Geochemistry and Geophysics, University of Bayreuth, Universitätsstr. 30, D-95440 Bayreuth, Germany

[⊥]Hamburger Synchrotronstrahlungslabor, Notkestr. 85, D-22603 Hamburg, Germany

ABSTRACT: Different modifications of Li_xMoO_2 (1) without metallic Mo−Mo bonds (R-3m, a = 2.858(2) Å, c = 15.701(13) Å), (2) with endless Mo chains with metallic bonds ($C2/m$, a = 10.614(3) Å, b = 2.878(1) Å, c = 4.955(2) Å, β = 99.37(3)°), and (3) with Mo_4O_{16} clusters ($C2/m$, a = 9.905(6) Å, b = 5.739(3) Å, c = 5.472(4) Å, β = 107.43(7)°) were synthesized by high-temperature solid-state reaction. Increasing lithium content supports the formation of the rhombohedral form. In situ structural investigations during electrochemical Li extraction and insertion between 2.4−3.5 V on $Li_{1.0}MoO_2$ material containing rhombohedral and monoclinic modifications with endless molybdenum chains revealed the instability of the monoclinic $Li_{0.9}MoO_2$ form with decreasing Li content against transformation into two rhombohedral phases Li_xMoO_2 and $Li_{x\approx0}MoO_2$. In contrast, the rhombohedral $Li_{1.0}(Mo_{0.9}Li_{0.1})O_2$ form showed a topotactical single-phase behavior during Li extraction and insertion. Further oxidation of Li_xMoO_2 at voltages above 4.5 V led to insertion of large anions such as PF_6^- or BF_4^- into the crystal structure. The Li-free rhombohedral form is stable in Ar up to 570 K and transforms irreversibly at higher temperature into a rutile-like structure.

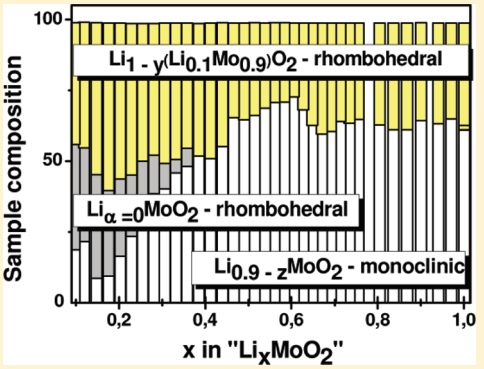

KEYWORDS: monoclinic Li_xMoO_2, rhombohedral Li_xMoO_2, Mo_4O_{16}-clusters, in situ structural characterization, lithium extraction/insertion, thermal stability

INTRODUCTION

Layered lithium molybdenum oxide $LiMoO_2$, isostructural to widely known $LiMO_2$ (M = Co, Mn, Ni, Fe) cathode materials for Li ion batteries, seems to offer promising characteristics as a potential Li storage material.[1] It can reversibly accommodate up to 0.85 Li per "MoO_2" unit at an average potential of 3 V[1] with an initial capacity of about 200 mAh/g.[2] Li_xMoO_2 demonstrates a high lithium mobility, which is dependent on the Li content x.[3] The simplified structural model of $LiMoO_2$ represents edge-sharing MoO_6 octahedra, which form MoO_2 layers with Li atoms between them. Lithium and molybdenum are ordered giving hexagonal sheets of Li(+1) and Mo(+3) in alternate layers. The information about structural details is contradictory. There are two crystallographic modifications of Li_xMoO_2 with very similar structural motives, monoclinic and rhombohedral ones. According to Aleandri et al.,[4] in rhombohedral Li_xMoO_2 (R-3m) each Mo atom is bonded to six other Mo atoms in a hexagonal sheet with d(Mo−Mo) = 2.866 Å, which is longer than the Mo−Mo bond length in metallic Mo (2.72 Å). In the monoclinic form of Li_xMoO_2 ($C2/m$), Mo ions are distorted from an ideal hexagonal array toward neighboring Mo atoms with bond distances of 2.881 Å between adjacent Mo atoms of the same row and of 2.549 Å between Mo atoms of adjoining rows, so that zigzag metallic Mo−Mo bonds appear within the chains.[5] According to a theoretically predicted instability of hexagonal sheets against the formation of either zigzag chains or chain clusters[5] for d^3 electronic systems, $LiMoO_2$ with Mo(III) should be monoclinic with metallic Mo−Mo bonds. Increasing of the average Mo oxidation state through Li excess in the structure in comparison to Mo and, therefore, a mixed Li/Mo occupancy in (MoO_2)-layers should stabilize the rhombohedral symmetry. The similarity of the ionic radii of Mo^{3+}/Mo^{4+} and Li^+ in oxygen octahedra promotes the existence of a solid solution with different Li/Mo ratios and random Li/Mo distribution on the Mo site, which was observed for example

Received: February 7, 2011
Revised: June 16, 2011
Published: July 11, 2011

in $Li_{1.0}(Li_{0.33}Mo_{0.67})O_2$, or Li_2MoO_3.[6,7] Taking into account the literature data, one can conclude a rhombohedral symmetry without metallic Mo−Mo bond for phases with excess Li over Mo in the structure, although, for example, the $Li_{0.74}MoO_2$ structure was described by monoclinic[1] and rhombohedral[2] symmetry.

The $P(O_2)$−T−x phase diagram of the Li−Mo−O system is missing, perhaps because of the complexity of the system due to high Li diffusion and the impossible precise determination of the Li content in each phase for multiphase samples by laboratory X-ray powder diffraction. Strong preferred orientation of crystallites perpendicular to layers makes the crystal structure solution from powder diffraction challenging. Most structural experiments were made on powdered samples, which were kept in air. It is known that layered structures can include water molecules between layers that significantly change crystallographic and physical properties. It was shown that Li-deficient Li_xMoO_2 materials undergo hydratation reactions leading to hydrate phases $Li_x(H_2O)_yMoO_2$.[1] The Li_2O−MoO_2 pseudobinary section has been investigated at 833 K:[8] the $LiMoO_2$ phase was not found at this temperature.

The similarity of $LiCoO_2$ and $LiMoO_2$ as cathode materials is often postulated due to the same crystal structure type, although there are more differences between these systems. First, Li_xCoO_2 with $x \leq 0.8$ has a tendency to release oxygen and transform into Co_3O_4,[9] whereas practically Li-free Li_xMoO_2 can be obtained electrochemically or by soft oxidation with Br_2 or I_2.[7] Second, the metallic Mo−Mo bonding in the Li_xMoO_2 polymorph should influence the resulting electrochemical properties in contrast to $LiCoO_2$ without metallic Co−Co bonds. Some works were devoted to electrochemical investigations of Li_xMoO_2,[1−3,8] but any detailed structural characterizations during Li extraction and insertion are lacking. Structural investigations[1] revealed a multiphase extraction/intercalation mechanism in Li_xMoO_2 over the composition range of 0.15−1.0 with some single phase regions.

Note that chemical or electrochemical lithiation of monoclinic rutil-type MoO_2 led to the filling of channels in the structure within the same structure type.[10]

In the present work, a detailed single crystal structural characterization of water-free lithium molybdenum oxides Li_xMoO_2 ($0.85 \leq x \leq 1.0$) with different Li contents, obtained by a high-temperature solid-state reaction, was performed. Crystal structures of Li_xMoO_2 ($0 < x \leq 1.0$) formed during electrochemical Li extraction and insertion in $Li_{1.0}MoO_2$ were investigated in situ by synchrotron diffraction and compared with structures obtained through chemical oxidation. Phase identification during Li extraction and intercalation will contribute to the understanding of the fatigue mechanism of Li_xMoO_2 during charge/discharge cycling in Li ion batteries and allows the prediction of the best Li_xMoO_2 composition as a cathode for electrochemical energy storage.

EXPERIMENTAL SECTION

Synthesis and Chemical Analysis. Li_xMoO_2 ($x = 0.85, 0.90, 1.0$) samples were prepared by solid-state reaction from stoichiometric amounts of Li_2MoO_4 (Alfa Aesar, 99%), Mo (Alfa Aesar, 99.95%), and MoO_3 (Alfa Aesar, 99.95%) placed in Al_2O_3 crucibles in evacuated and sealed silica tubes at 1223 K during 20 h according to the following reactions 1−3.

$$Li_2MoO_4 + Mo \rightarrow 2Li_{1.0}MoO_2 \quad (1)$$

$$0.9Li_2MoO_4 + 0.97Mo + 0.13MoO_3 \rightarrow 2Li_{0.9}MoO_2 \quad (2)$$

$$0.85Li_2MoO_4 + 0.95Mo + 0.2MoO_3 \rightarrow 2Li_{0.85}MoO_2 \quad (3)$$

$$LiMoO_2 + NO_2BF_4 \rightarrow [MoO_2] + NO_2 + LiBF_4 \quad (4)$$

$$LiMoO_2 + \tfrac{1}{2}NO_2BF_4 \rightarrow Li_{0.5}MoO_2 + \tfrac{1}{2}NO_2 + \tfrac{1}{2}LiBF_4 \quad (5)$$

The synthesis conditions of reactions 1−3 led to the formation of Li_xMoO_2 single crystals. The Li content in Li_xMoO_2 for $x \leq 0.85$ was reduced by two different methods: a chemical reaction at room temperature under Ar atmosphere in acetonitrile medium between Li_xMoO_2 powder and nitronium tetrafluoroborate, NO_2BF_4, as an oxidizing agent, according to the reactions 4−5, or in electrochemical cells. For the synthesis with NO_2BF_4, it was mixed with $Li_{1.0}MoO_2$ in molar ratio 1/1 or 0.5/1. A sufficient amount of acetonitrile was added to obtain a liquid mixture. After syntheses with NO_2BF_4, Li_xMoO_2 ($x \leq 0.85$), samples were washed with acetonitrile to remove traces of unreacted agents and dried under vacuum at room temperature. The amount of Li and Mo in all prepared Li_xMoO_2 compounds were determined quantitatively by the ICP-OES method (IRIS Intrepid II XUV, Thermo Fisher) using a 3:1 mixture of HCl (37%, p.a. Fa. Merck) and HNO_3 (65%, p.a. Fa. Merck) for dissolving the samples.

Structural Characterization and Phase Analysis. The crystal structures of Li_xMoO_2 were solved by single-crystal X-ray diffraction using the Xcalibur system from Oxford Diffraction. The software packages SHELXS[11] and SHELXL[12] were used for structure solution and refinement as included in X-STEP32.[13] A combined empirical absorption correction with frame scaling was applied, using the SCALE3 ABSPACK command in CrysalisRed.[14] Phase analysis and determination of cell parameters of Li_xMoO_2 at room temperature were carried out using X-ray powder diffraction (XPD) with a STOE STADI P diffractometer (Cu $K\alpha_1$ radiation, $\lambda = 1.54059$ Å) in transmission mode. Diffraction experiments for phase analyses of the Li_xMoO_2 materials with $x \leq 0.85$ after electrochemical treatments or chemical oxidizing were performed without any contact of the sample with air.

Structural analysis of the composition "$Li_{1.0}MoO_2$" after solid-state reaction, which was taken for in situ investigations during electrochemical Li extraction and insertion, was performed also by neutron powder diffraction at 3 and 300 K at the powder diffractometer SPODI[15] at the neutron research reactor FRM-II in Garching near Munich (Germany) with monochromatic neutrons of 1.5481(1) Å wavelength.

High-Temperature Structure Investigations. High-temperature structure investigations of Li_xMoO_2 powders in Ar between 295 and 1173 K in temperature steps of 20 or 30 K have been performed by synchrotron diffraction at HASYLAB/DESY (Hamburg, Germany) at beamline B2[16] in Debye−Scherrer mode using the on-site readable image plate detector OBI[17] and a STOE furnace equipped with a EUROTHERM temperature controller and a capillary spinner. The 0.3 mm quartz capillaries were filled with powdered Li_xMoO_2 in a glovebox under Ar-atmosphere, sealed, and mounted inside the STOE furnace. The wavelength of 0.49962(1) Å was selected by a double-crystal monochromator and determined from the positions of eight reflections from a LaB_6 reference material. Before being measured, a $Li_{x\approx 0}MoO_2$ sample after chemical Li extraction was washed with acetonitrile and dried in vacuum at room temperature.

Electrochemical Characterization. Electrochemical studies on a $Li_{1.0}MoO_2$ cathode were performed with a multichannel potentiostatic−galvanostatic system VMP3 (Bio-Logic) in standard Swagelok-type cells with metallic Li as the anode material. For the positive electrode, a mixture of $Li_{1.0}MoO_2$, carbon black, and polyvinylidene fluoride (PVDF) as a polymer binder in an 80:10:10 weight ratio was pressed on Al meshes with 8 mm diameter and dried in vacuum at 373 K. A 1 M solution of $LiPF_6$ in a mixture of ethylene carbonate (EC) and dimethylcarbonate (DMC) (1:1) was used as the electrolyte. The cells were assembled in an Ar-filled glovebox with H_2O and O_2 contents less than 1 ppm.

In Situ Structural Investigations during Li Insertion and Extraction. In situ X-ray synchrotron diffraction measurements on $Li_{1.00}MoO_2$ were performed at the synchrotron facility HASYLAB/DESY (Hamburg, Germany) at beamline B2 in transmission mode using

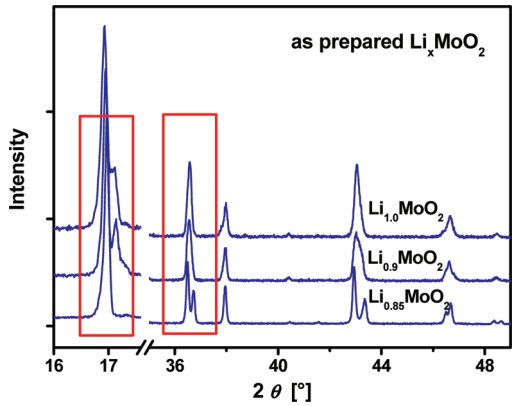

Figure 1. X-ray powder diffraction patterns (Cu $K\alpha_1$ radiation, λ = 1.54059 Å) of Li_xMoO_2 with x = 0.85, 0.9, and 1.0 compositions, prepared by solid-state reaction. In spite of the common similarities, the crystal structure of $Li_{0.85}MoO_2$ differs from x = 0.9 and 1.0; the strongest differences are marked by frames.

the on-site readable image plate detector OBI and a cell connected to a VMP multichannel galvanostat.[18] A Swagelok-type in situ cell for battery investigations using synchrotron radiation was taken.[19] As cathode material, a mixture of $Li_{1.0}MoO_2$, PVDF and carbon black (80/10/10 weight ratio) of 40 mg was used. Data were collected in steps of 0.004° over the 2θ range from 4° to 55°; the wavelength of 0.62850(1) Å was determined from the positions of eight reflections from a LaB_6 reference material.

To characterize the starting material $Li_{1.00}MoO_2$, a pattern was recorded before the electrochemical process was started. The cell was then successively charged and discharged in galvanostatic mode at a constant current corresponding to the intercalation or deintercalation of 1 Li per formula unit during 10 h (C/10 rate). All diffraction patterns have been analyzed using the software package WinPLOTR. The Al foil as the current collector on the cathode side served as an internal standard during the measurements, and the refined lattice parameter of Al provided an independent control of the reliability of the obtained model parameters.

X-ray Photoelectron Spectroscopy (XPS). X-ray photoelectron spectroscopy was applied on as prepared "$Li_{1.0}MoO_2$" and on the products with different lithium contents after electrochemical Li extraction and battery cycling. A PHI 5600 CI system with an Al Kα 350 W monochromatized X-ray source and a hemispherical analyzer at a pass energy of 29 eV were used. Cells with pellets of the same cathode mixture consisting of "$Li_{1.0}MoO_2$", carbon black, and PVDF with a mass of about 30 mg were charged to x(Li) $\approx$ 0.6, 0.4, and 0.0, or 30 times cycled and immediately disassembled in the glovebox. Two different electrolyte salts, $LiPF_6$ and lithium bis(oxalate)borate LiBOB, were used. In order to remove the electrolyte from the surface, the pellets were washed with DMC and scraped. After drying, the samples were transferred from the glovebox to the XPS system in an Ar-filled transfer chamber performing in this way a quasi in situ XPS analysis.[20] During XPS measurements, when necessary, surface charging was minimized by means of a low-energy electron flood gun. The system base pressure was about 10^{-9} mbar. The binding energy scale was calibrated from minor carbon contaminations using the C1s peak at 284.8 eV.

RESULTS

1. Synthesis and Crystal Structure Determination of Li_xMoO_2 Obtained by a Solid-State Route. Three different compositions, "$LiMoO_2$", "$Li_{0.9}MoO_2$", and "$Li_{0.85}MoO_2$", were obtained by solid-state reaction in evacuated sealed silica tubes at 1223 K, following slow cooling to room temperature. After all syntheses, the silica tubes appeared opaque, indicating some

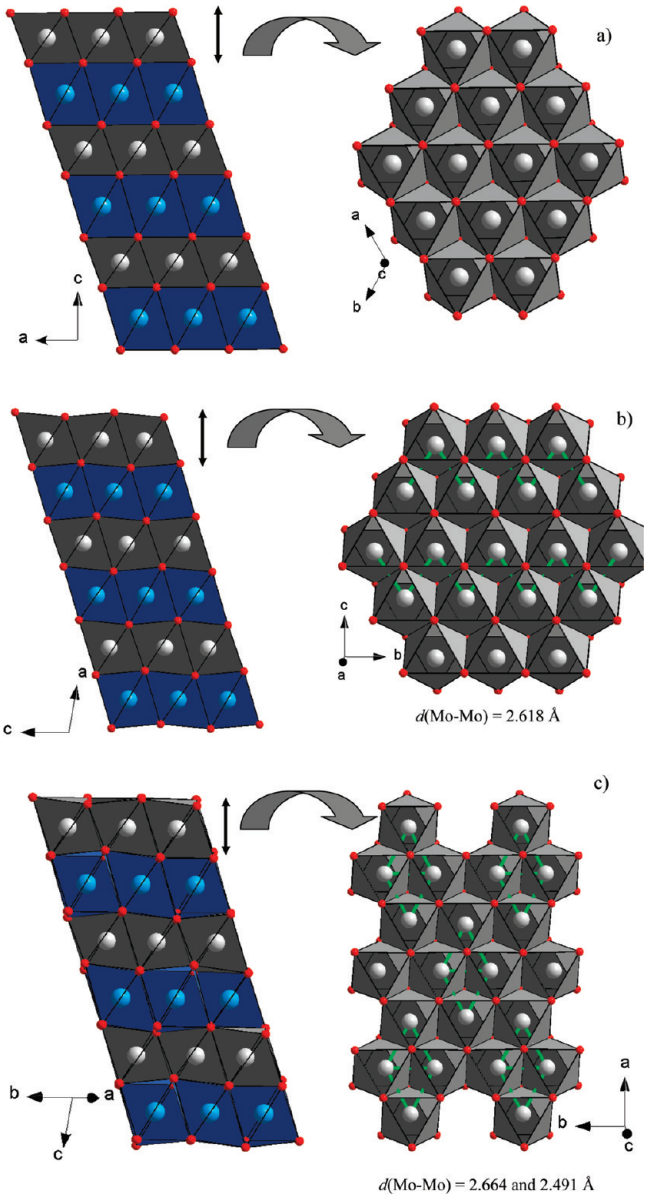

Figure 2. Three different crystal structures of Li_xMoO_2 obtained after the synthesis by solid-state reaction in evacuated quartz tubes: (a) rhombohedral form with Mo−Mo bonds of 2.869 Å longer than in metallic Mo (2.72 Å), (b) monoclinic form with endless Mo chains forming metallic Mo−Mo bonds, and (c) monoclinic form with finite Mo_4O_{16} clusters forming shorter and longer metallic bonds.

reaction with the samples, probably some inclusion of Li. ICP-OES results after chemical analysis revealed a slight Li deficiency of 3−4% for the compositions, for example, $Li_{0.97(3)}Mo_{1.0}O_2$ instead of $LiMoO_2$ and $Li_{0.82(2)}MoO_2$ instead of $Li_{0.85}MoO_2$. Comparison of X-ray powder diffraction patterns for the three materials pointed out multiphase samples with similar structures for "$LiMoO_2$" and "$Li_{0.9}MoO_2$" compositions, whereas "$Li_{0.85}MoO_2$" could be a single-phase sample with much stronger crystal structure distortion (Figure 1). XRD patterns of Li_xMoO_2 for x = 1.0 and 0.9 were satisfactorily explained in assumption of a mixtures of known $LiMoO_2$ rhombohedral[4] and $Li_{0.75}MoO_2$ monoclinic[1] forms, mainly due to the presence of two reflections around 2θ of 17°. Attempts to refine the same structural model, based on the

dx.doi.org/10.1021/cm2010715 |Chem. Mater. 2011, 23, 3429–3441

Table 1. Details of X-ray Single-Crystal Data Collection and Structure Refinement of Li_xMoO_2[a]

chemical formula	$Li_{1.0}MoO_2$	$Li_{0.91}MoO_2$	$Li_{0.75}MoO_2$
formula weight	134.88	134.71	133.15
crystal system, space group	rhombohedral, *R*-3*m*	monoclinic, *C*2/*m*	monoclinic, *C*2/*m*
unit cell dimensions	a = 2.858(2) Å, c = 15.701(13) Å	a = 9.905(6) Å, b = 5.739(3) Å, c = 5.472(4) Å, β = 107.43(7)°	a = 10.614(3) Å, b = 2.878(1) Å, c = 4.955(2) Å, β = 99.37(3)°
cell volume (Å^3)	111.04(14)	296.8(3)	149.34(9)
Z, calculated density (g/cm^3)	3, 6.051	8, 6.038	4, 5.999
radiation type		Mo Kα, λ = 0.71073 Å	
temperature (K)	293(2)	293(2)	293(2)
crystal form, color	prismatic, black	prismatic, black	prismatic, black
crystal size (mm^3)	0.07 × 0.04 × 0.01	0.055 × 0.035 × 0.015	0.01 × 0.30 × 0.01
data collection			
diffractometer: Oxford Diffraction Xcalibur, single-crystal X-ray diffractometer with sapphire CCD detector			
data collection method: rotation method data acquisition using ω and φ scans(s)			
absorption coefficient (mm^{-1})	8.287	8.268	8.215
F(000)	183	488	244
theta range for data collection	3.89 to 28.72°	3.90 to 29.70°	3.89 to 29.70°
range of h, k, l	$-3 \le h \le 3$, $-3 \le k \le 2$, $-21 \le l \le 20$	$-9 \le h \le 13$, $-7 \le k \le 7$, $-7 \le l \le 6$	$-14 \le h \le 14$, $-3 \le k \le 3$, $-6 \le l \le 6$
reflections collected/unique	140/53 [R(int) = 0.0486]	667/403 [R(int) = 0.0552]	562/233 [R(int) =0.0244]
completeness to theta = 26.3° (0.8 Å)	100%	94.6%	99.5%
refinement method: full-matrix least-squares on F^2			
data/restraints/parameters	53/0/9	403/0/25	233/0/30
goodness-of-fit on F^2	1.308	1.016	1.107
final R indices [I > 2sigma(I)]	R_1 = 0.0399, wR_2 = 0.0990	R_1 = 0.0542, wR_2 = 0.1173	R_1 = 0.0232, wR_2 = 0.0535
R indices (all data)	R_1 = 0.0396, wR_2 = 0.0990	R_1 = 0.1092, wR_2 = 0.1425	R_1 = 0.0258, wR_2 = 0.0556
largest diff. peak and hole	1.798 and −1.353 e/Å^3	2.100 and −2.435 e/Å^3	1.800 and −1.430 e/Å^3

[a] Li content was determined from structural refinements.

diffraction data of $Li_{0.85}MoO_2$ or only using structure data from each modification, gave a large discrepancy between observed and calculated curves.

Analysis of X-ray single crystal diffraction data for these three Li_xMoO_2 compositions revealed the existence of two monoclinic and one rhombohedral modification of Li_xMoO_2 with layered structures and different Li/Mo ratios (Figure 2 and Tables 1 and 2). The differences between crystal structures included a distortion of MO_6 octahedra, different types of Mo cluster formations in molybdenum layers, and Li stoichiometry. Li content in the rhombohedral and one monoclinic form were refined also from neutron powder diffraction for $LiMoO_2$ composition.

The rhombohedral *R*-3*m* modification represents the structure with the highest degree of order and a minimal distortion of the MO_6 octahedra. No Mo_xO_y clusters (Figure 2a) are formed because no metallic Mo−Mo bonds exist, which would result in Mo−Mo distances shorter than in metallic molybdenum (2.72 Å). According to single crystal analysis, a composition $Li_{1.0}MoO_2$ can be concluded with Mo atoms on the 3*a* site and Li atoms on the 3*b* site. Similarity of ionic radii of Mo^{3+}/Mo^{4+} and Li^+ in oxygen octahedra provide a mixed Li/Mo occupancy, which was observed, for example, in Li_2MoO_3.[7]

Actually, the structure refinement based on neutron diffraction data gave some Li excess over Mo concentration in the phase: Li layers alternate with molybdenum−lithium layers, in which Li and Mo atoms are randomly distributed. Therefore, the composition of the rhombohedral form in the "$Li_{1.0}MoO_2$" sample can be written as $Li(Li_{0.11(1)}Mo_{0.89(1)})O_2$. Structural features of $Li(Li_{0.11(1)}Mo_{0.89(1)})O_2$ are similar to the ones of Li_2MoO_3, or $Li(Li_{0.33}Mo_{0.67})O_2$ reported in work.[7]

Structure refinement of the monoclinic modification *C*2/*m* with lattice parameters a = 10.614(3) Å, b = 2.878(1) Å, c = 4.955(2) Å, β = 99.37(3)° (Tables 1 and 2) based on neutron powder diffraction gave a strong correlation between Li thermal displacement parameters and site occupancies. For example, a relatively large thermal parameter of 1.78 Å^2, constrained to the same value for both lithium sites 2*b* and 2*c*, was refined for a fixed full occupation on both Li sites at room temperature. If the thermal displacement is fixed at 1.00 Å^2 instead, a small Li deficiency on both Li sites is refined and results in the $Li_{0.92(2)}MoO_2$ composition. Single-crystal diffraction provided more Li deficiency in the structure, namely $Li_{0.75}MoO_2$. The structure has endless chains of Mo atoms (Figure 2b) with a metallic Mo−Mo bond length of 2.618 Å within Mo layers. A similar crystal structure was described for $Li_{1.33}Mo_2O_4$, obtained by a soft ionic exchange method from a Na-containing molybdate.[1]

Another monoclinic modification, found in the $Li_{0.85}MoO_2$ sample, is characterized by the strongest octahedral distortion among the rhombohedral and known monoclinic Li_xMoO_2 forms and the formation of finite rhombohedron-like Mo_4O_{16} clusters with metallic Mo−Mo bonds with distances d(Mo−Mo) of 2.664 and 2.491 Å (Figure 2c and Tables 1, 2). Single-crystal diffraction gave the stoichiometry $Li_{0.91(3)}MoO_2$, if all Li thermal displacement parameters are constrained to the same value. In the Inorganic

dx.doi.org/10.1021/cm2010715 |*Chem. Mater.* 2011, 23, 3429–3441

Table 2. Atomic Coordinates and Equivalent Isotropic Displacement Parameters (Å^2) for Li_xMoO_2

$Li_{1.0}MoO_2$ *R*-3*m*						
atom	site	*x*	*y*	*z*	occup.	U(eq)
Mo(1)	3*a*	0	0	0	1	0.019(1)
O(1)	6*c*	0	0	0.0808(8)	1	0.012(3)
Li(1)	3*b*	0.6667	0.6667	0.1667	1	0.03(2)
$Li_{0.91}MoO_2$ *C*2/*m*						
atom	site	*x*	*y*	*z*	occup.	U(eq)
Mo(1)	4*h*	0.5	0.7169(3)	0.5	1	0.014(1)
Mo(2)	4*i*	0.2616(2)	0.5	0.4959(4)	1	0.019(1)
O(1)	4*i*	0.616(1)	1.0	0.706(2)	1	0.004(3)
O(2)	4*i*	0.371(2)	0.5	0.235(3)	1	0.016(3)
O(3)	8*j*	0.376(1)	0.754(1)	0.753(2)	1	0.013(3)
Li(1)	2*b*	0.5	1.0	1.0	1	0.027(6)
Li(2)	4*e*	0.25	0.25	0	1	0.027(6)
Li(3)	2*a*	0.5	0.5	0	0.66(14)	0.027(6)
$Li_{0.75}MoO_2$ *C*2/*m*						
atom	site	*x*	*y*	*z*	occup.	U(eq)
Mo	4*i*	0.2520(1)	0.5	0.2142(1)	1.0	0.009(1)
O(1)	4*i*	0.1180(4)	0.5	−0.1358(9)	1.0	0.007(1)
O(2)	4*i*	0.1433(4)	0	0.3819(9)	1.0	0.009(1)
Li(1)	2*b*	0	0.5	−0.5	0.9(1)	0.032(10)
Li(2)	2*c*	0	0	0	0.6(1)	0.018(11)

Crystal Structure Database (ICSD)[21] no other compounds are included, which adopt this $Li_{0.9}MoO_2$ structure with similar parameters.

Because of the missing Li−Mo−O phase diagram at 1100−1200 K,[8] it is impossible to discuss the thermodynamic stability of the different modifications and their Li content as a function of temperature. Synthesis of "$LiMoO_2$" composition at 1223−1273 K gave always a phase mixture of monoclinic and rhombohedral forms with some differences in Li content (Figure 3), which should be dependent on synthesis temperature and cooling rate. Some Li deficiency causes the distortion of Mo−O layers and the appearance of longer and shorter Mo−Mo distances, so that a formation of Mo chains with metallic bonds occurs. Dedicated synthesis of Li-deficient phases lead to the appearance of the other monoclinic form with a more pronounced structure distortion and isolated Mo_4O_{16} clusters with longer and shorter metallic bonds inside. It is expected that each structural modification $Li_x(Mo_{1-y}Li_y)O_2$ exhibits a significant Li nonstoichiometry.

2. High-Temperature Structure Investigations of $Li_{1.0}MoO_2$ Sample. As-prepared $Li_{1.0}MoO_2$ sample was investigated during heating in Ar by synchrotron powder diffraction, see Figure 4. The appearance of Li_2MoO_4 reflections between 520 and 970 K (Figure 4) together with the nonlinearity of temperature dependences of lattice parameters for rhombohedral and monoclinic forms of Li_xMoO_2 at these temperatures (Figure 5) indicate a rearrangement of the cations in lithium molybdates during increasing temperature, supporting a high lithium mobility in these phases at elevated temperature.

3. In Situ Structural Investigations of "$Li_{1.0}MoO_2$" during Electrochemical Lithium Extraction and Insertion between 2.0 and 4.0 V. Structural changes during electrochemical lithium extraction down to 15% residual Li and reinsertion were studied by in situ synchrotron diffraction on the pristine material with "$Li_{1.0}MoO_2$" stoichiometry, containing a mixture of rhombohedral (28% w/w) and monoclinic (71% w/w) forms of Li_xMoO_2 with endless Mo chains in the structure (Figure 3c) and less than 1% (w/w) metallic Mo. Neutron diffraction of the sample indicated the $Li(Li_{0.11}Mo_{0.89})O_2$ composition for the rhombohedral modification, and $Li_{0.92}MoO_2$ for the monoclinic one, see previous section. A PCGA (Potentiodynamic Cycling with Galvanostatic Acceleration) experiment performed on the same with I_{lim} close to C/20 (ΔE = 5mV) showed some complex electrochemical processes between 2.0 and 4.0 V, which are similar to the data observed in work[2] for $LiMoO_2$, revealing the multiphase extraction−insertion mechanism (Figure 6). Galvanostatic cycling with potentiostatic limitation (GCPL) between 2.8 and 3.7 V with C/10 corresponds to extraction/insertion of about 0.9 Li per $LiMoO_2$ (Figure 6).

An overview of diffraction patterns collected at different Li contents revealed a reversible character of Li extraction and insertion (Figure 7). One intermediate phase appears below x = 0.36 during Li extraction and disappeared above x = 0.36 following Li insertion. Its crystal structure can be described on the basis of the pristine rhombohedral unit cell with longer *a*- and somewhat shorter *c*-parameter in comparison with the initial unit cell. The amount of metallic Mo (about 1%w/w) remains constant during the whole extraction−insertion process, while the amounts of other phases change (Figure 8).

From x = 1.0 down to x = 0.65 in Li_xMoO_2 the amounts of the monoclinic and rhombohedral forms remain nearly constant (Figure 8). Below x = 0.65, the amount of the monoclinic modification slightly increases followed by a drastic decrease. At the same time, a new phase with the same rhombohedral symmetry but different lattice parameters appears, and the amount of the initial rhombohedral phase increases. From the GCPL experiment one can conclude that the large plateau between x = 0.35 and 0.15, corresponding to the oxidative peak at 3.25 V and reductive one at 3.38 V (Figure 6) in PCGA measurements, reflects a multiphase transformation of monoclinic Li_xMoO_2 into two rhombohedral phases with different lattice parameters. Synchrotron powder diffraction allows for very precise determination of the cell parameters but cannot define the specific lithium content reliably. The assumed nearly zero Li content in the new $Li_{x=0}MoO_2$ phase is supported by the practically constant lattice parameters (Figure 11), while the total lithium content in the sample changed. Refinement of the cation occupancy in the new phase gave unambiguously only Mo atoms on the 3*a* site. Analysis of Mo/Li mixed occupancy on the 3*a* site in the pristine rhombohedral form (89% of Mo in pristine composition) revealed practically no changes within standard deviations during charge/discharge, so that a topotactical Li extraction and insertion from or on the 3*b* site can be proposed for rhombohedral modification $Li(Li_{0.11}Mo_{0.89})O_2$. The transformation of the Li-deficient monoclinic form into two rhombohedral phases should be caused by instability of metallic zigzag Mo-chains against a Mo-network without metallic bonding. Theoretical DFT calculations of the electronic structure are needed to evaluate the most stable constitution.

The lattice parameters change in the monoclinic and rhombohedral forms in a nonmonotonous (Figures 9 and 10) way and

dx.doi.org/10.1021/cm2010715 |*Chem. Mater.* 2011, 23, 3429–3441

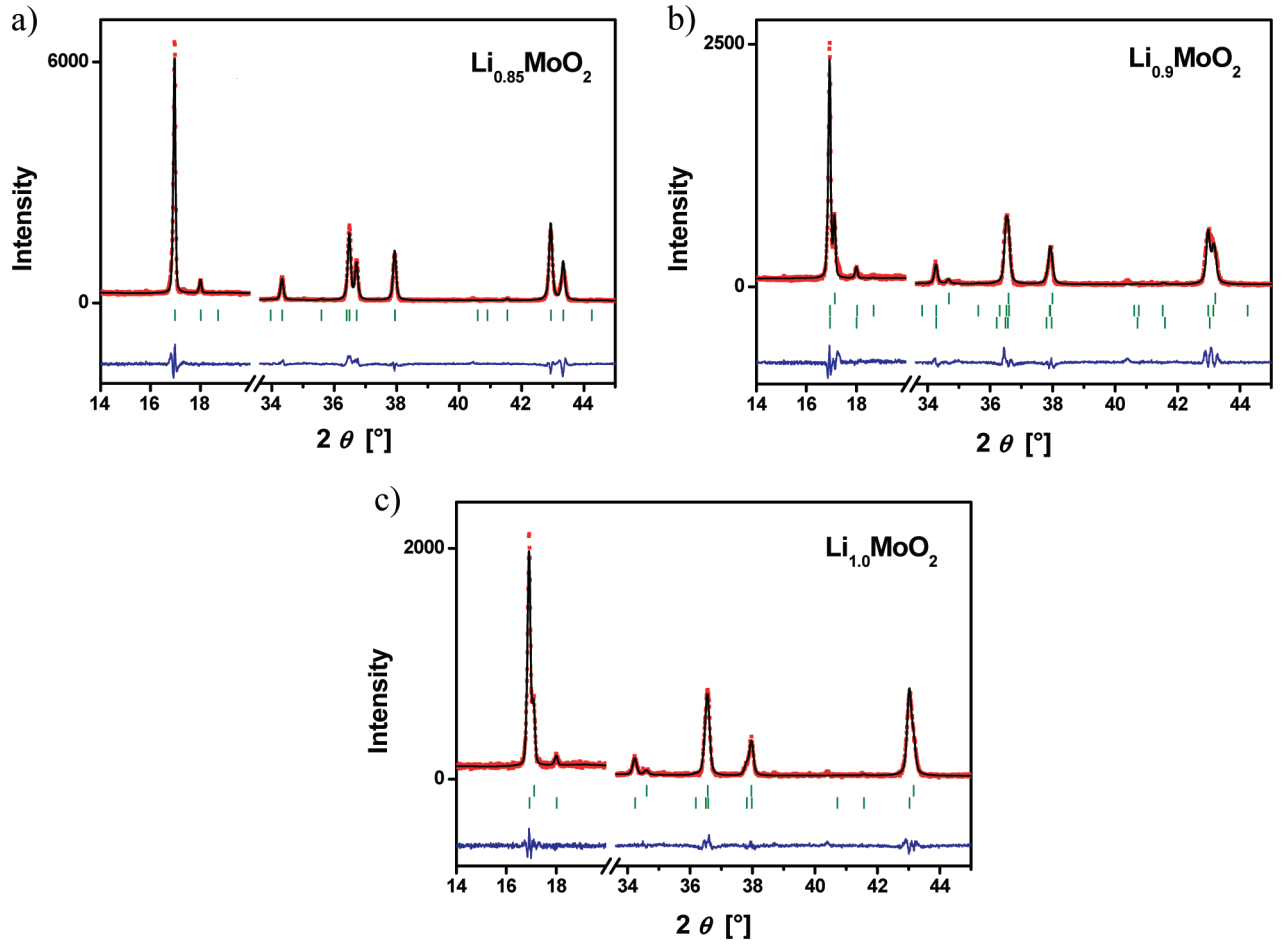

Figure 3. Sections of the measured (Cu Kα_1 radiation, λ = 1.54059 Å) and calculated powder diffraction patterns for Li_xMoO_2 compositions, together with the difference curves, based on the following models. (a) $Li_{0.85}MoO_2$, *C*2/*m*, *a* = 9.91667(8) Å, *b* = 5.75667(5) Å, *c* = 5.46054(6) Å, β = 107.1217(6)°. (b) $Li_{0.9}MoO_2$, from top to bottom: *R*-3*m*, 19% (w/w), *a* = 2.86932(9) Å, *c* = 15.5065(5) Å *C*2/*m*, 65% (w/w); *a* = 9.9397(3) Å, *b* = 5.7484(2) Å, *c* = 5.4773(2) Å, β = 107.368(2)° *C*2/*m*, 15% (w/w) *a* = 10.5932(9) Å, *b* = 2.8662(4) Å, *c* = 4.9846(4) Å, β = 99.207(8)°. (c) $Li_{1.0}MoO_2$, from top to bottom: *R*-3*m*, 27% (w/w) *a* = 2.87121(7) Å, *c* = 15.5347(5) Å *C*2/*m*, 73% (w/w) *a* = 10.6022(3) Å, *b* = 2.86527(6) Å, *c* = 4.9830(1) Å, β = 99.200(2)°.

indicate a complex relationship between Li content and crystal structure, probably due to changes in the electronic structures beyond a rigid-band model like in Li_xCoO_2 (Figures 9, 10, and 11). As long a rigid-band model applies, only minor structural changes are accompanied and only electronic levels of one transition metal orbital species are involved in oxidation and reduction. At higher oxidation level, like for example in Li_xCoO_2 for $x < 0.5$, oxygen levels are also involved. This results in pronounced changes in the crystal and electronic structures.[22]

Generally, during Li extraction from layered Li_xMoO_2, two effects contribute to the resulting cell parameters changes: (1) repulsive forces between negatively charged Mo−O layers, leading to increasing the distance between layers, and (2) geometrical contraction of interlayer distance due to Li removing. At small Li deficiency, the repulsive forces between negatively charged neighboring Mo−O layers dominate, while at high Li deficiency the negative charge of Mo layers decreases because of increasing the average oxidation state of Mo. Therefore, a nonlinear dependence of lattice parameters on Li content in the phase can be expected. For the monoclinic form, the alternating sequence of Li_xO_6 octahedra layers and MoO_6 octahedra layers is running along the *a*-axis, and the interlayer distance shows a

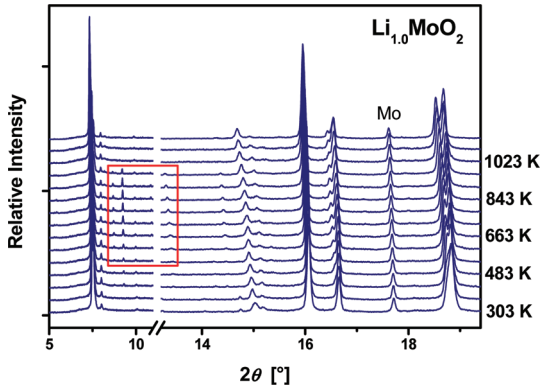

Figure 4. In situ thermal stability investigations in Ar by synchrotron diffraction on $Li_{1.0}MoO_2$ obtained by solid-state reaction at 1223 K. Li_2MoO_4 (melting point at 978 K) as intermediate phase appears between 520 and 960 K; the ranges with most characteristic reflections are marked by the frame.

pronounced maximum at $x = 0.7$, which correlates with a plateau in the GCPL at $0.8 \leq x \leq 1.0$. Note that this *x*-value corresponds

dx.doi.org/10.1021/cm2010715 |*Chem. Mater.* 2011, 23, 3429–3441

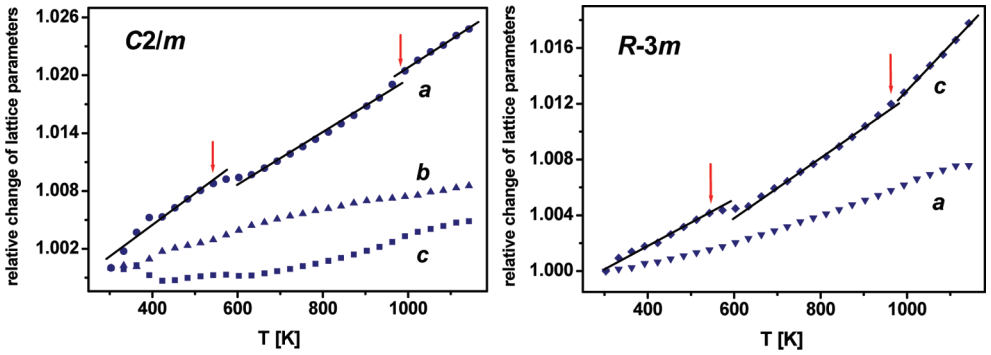

Figure 5. Lattice parameters for monoclinic (left) and rhombohedral (right) modifications of the $Li_{1.0}MoO_2$ sample, normalized to their 295 K values. Note that the observed changes in the *a*-parameter for the monoclinic form and the *c*-parameter for the rhombohedral one, which are sensitive for the interlayer distances, demonstrate a nonmonotonous behavior between 530 and 980 K, and the formation of Li_2MoO_4 was observed in this temperature range.

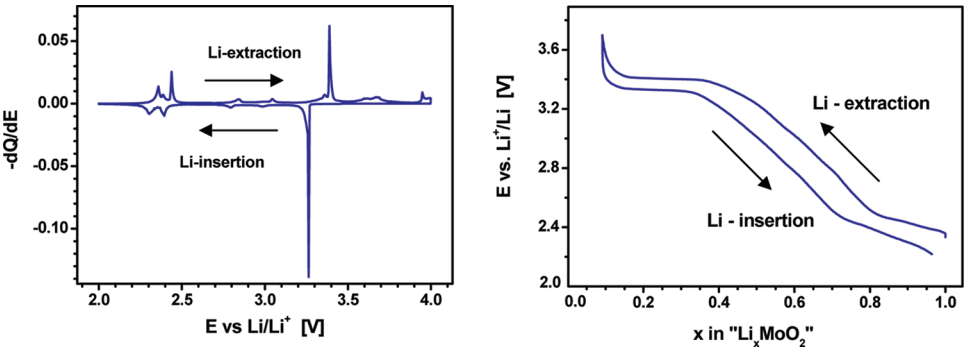

Figure 6. Electrochemical behavior (potentiodynamic cycling with I_{lim} close to C/20 (ΔE = 5mV) left and galvanostatic cycling with C/10 right) of the "$Li_{1.0}MoO_2$" sample, investigated in situ by synchrotron diffraction.

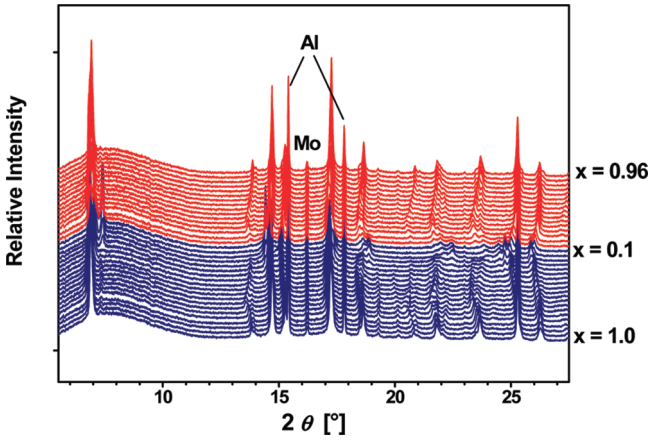

Figure 7. In situ synchrotron diffraction data from $Li_{1.0}MoO_2$ as cathode material in an electrochemical test cell with Li anode during CCPL at C/10. Blue: the cell was charged up to 4.1 V, which corresponds to the overall composition "$Li_{0.1}MoO_2$". Red: the cell was discharged down to 2.3 V and "$Li_{0.96}MoO_2$".

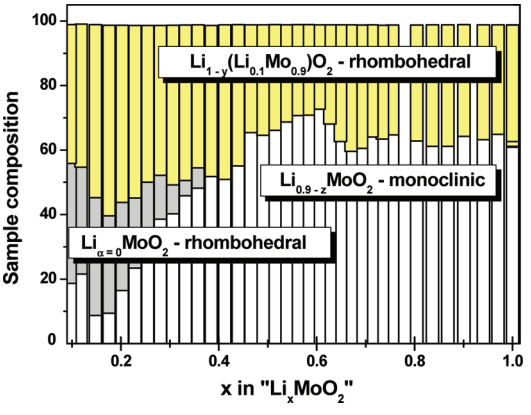

Figure 8. Relative amounts of Li_xMoO_2 phases with different structural symmetries during electrochemical Li extraction and insertion. Note that within each phase the specific Li content (α, *y*, *z*) can change but cannot be determined precisely from synchrotron diffraction and are therefore not quantified.

to the total Li content in the sample and can differ from the specific Li contents in the rhombohedral and monoclinic phases. Initially ($x \leq 1$), the *c*-axis decreases slightly, but increases from $x = 0.7$, whereas the *b*-axis increases to very low values of $x \sim 0.2$. Both the *b*- and *c*-axes reflect the intralayer Mo−Mo distance. During Li extraction, Mo atoms become more oxidized and, therefore, both Mo−Mo bonding and electron repulsion become weaker. Because of the much smaller changes in lattice parameters of the rhombohedral unit cell at the early stage of delithiation, the plateau in the GCPL at $0.8 \leq x \leq 1.0$ and the two signals in PCGA at 2.35 and 2.45 V may reflect changes in the electronic structure of the monoclinic form. For the rhombohedral form, the *c*-axis corresponds to the alternating sequence of Li_xO_6 octahedra layers and MoO_6 octahedra layers and shows a distinct maximum at $x = 0.5$, while the *a*-axis increases below $x = 0.7$ during Li extraction.

The present results do not support the model, proposed by James et al[7] about disproportionation of oxidized "Mo_3O_{13}"

dx.doi.org/10.1021/cm2010715 |*Chem. Mater.* 2011, 23, 3429–3441

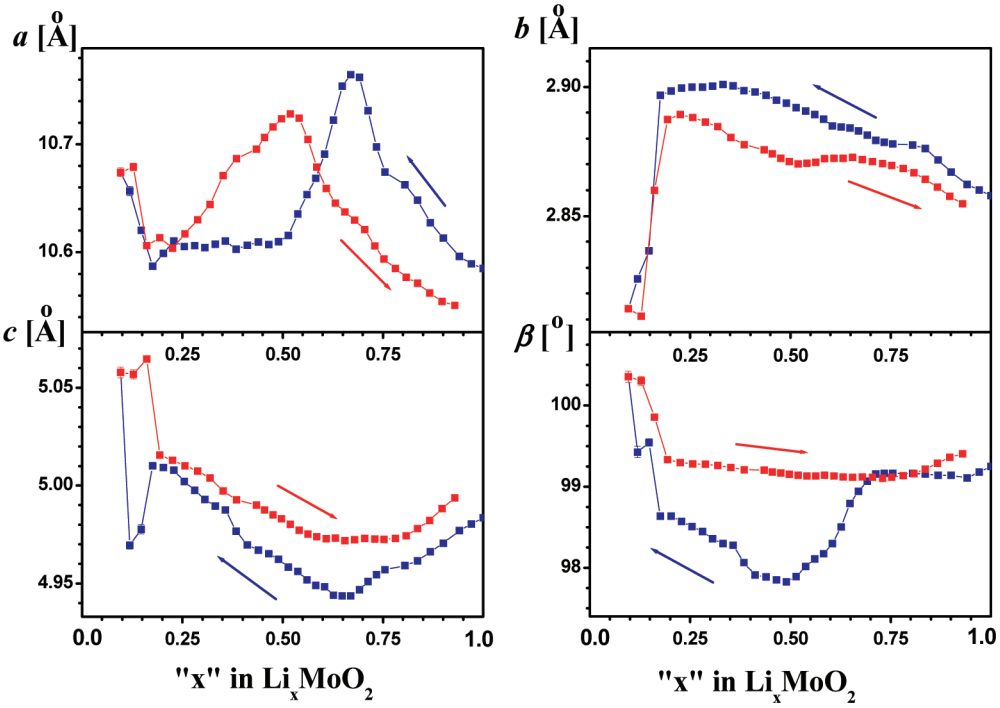

Figure 9. Changes in lattice parameters of monoclinic Li_xMoO_2 during in situ electrochemical Li extraction (blue) and insertion (red) from/in "$Li_{1.0}MoO_2$" composition. A complicated but reversible process can be concluded from the nonmonotonous evolution.

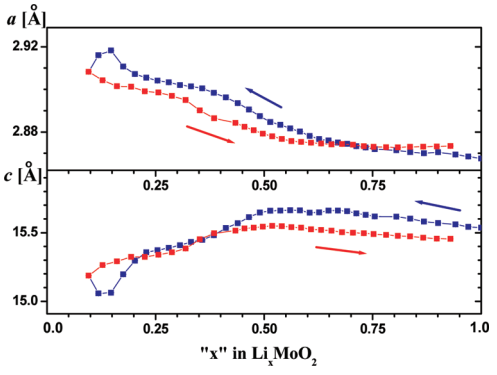

Figure 10. Changes in lattice parameters of rhombohedral Li_xMoO_2 during in situ electrochemical Li extraction and insertion from and in "$Li_{1.0}MoO_2$".

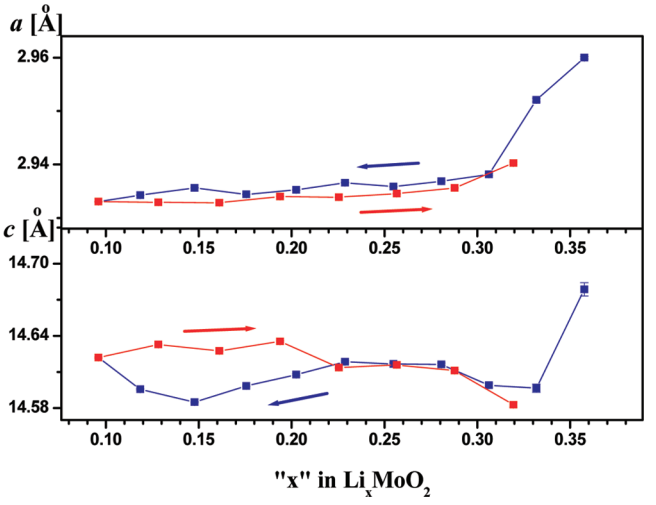

Figure 11. Changes in lattice parameters of the intermediate rhombohedral "$Li_{x\approx0}MoO_2$" phase during in situ electrochemical Li extraction and insertion.

clusters in Li_2MoO_3 to give isolated Mo^{6+} ions, which migrate to electrostatically favoured sites vacated by lithium in the successive layers, and, hereby, decrease the c/a ratio in $Li_{2-x}MoO_3$. On one hand, in situ synchrotron diffraction data are in agreement with such a mechanism because below $x = 0.5$ the c/a ratio of Li_xMoO_2 becomes smaller. On the other hand, the observed intensities do not indicate any Mo atoms in Li layers.

Below an overall Li content in the samples of "x" = 0.15 the monoclinic form trends to disappear, and its lattice parameters demonstrate drastic changes pointing out that this phase is only metastable at these conditions.

4. Oxidation of $Li_{1.0}MoO_2$ at High Electrochemical Potentials: Structural Considerations. *4.1. Electrochemical Oxidation of $Li_{1.0}MoO_2$.* In order to remove Li completely from the Li_xMoO_2 structure, and to study the stability of Mo(IV) species at high voltage the composition $Li_{1.0}MoO_2$, containing rhombohedral and monoclinic Li_xMoO_2 phases (Figure 3c), was oxidized chemically and electrochemically at potentials of 4.5−5.0 V against Li^+/Li. The formed phases were structurally characterized by X-ray powder diffraction. Multiphase samples were always observed after the oxidation. Similar to the results of in situ synchrotron diffraction during Li extraction from $Li_{1.0}MoO_2$ in the potential range of 2.4−3.7 V, electrochemical oxidation to $Li_{0.4}MoO_2$ and $Li_{x\approx0}MoO_2$ between 4.5 and 5 V revealed two rhombohedral modifications (R-3m) with different lattice parameters and one monoclinic phase ($C2/m$) for x = 0.4 and two

dx.doi.org/10.1021/cm2010715 |*Chem. Mater.* 2011, 23, 3429–3441

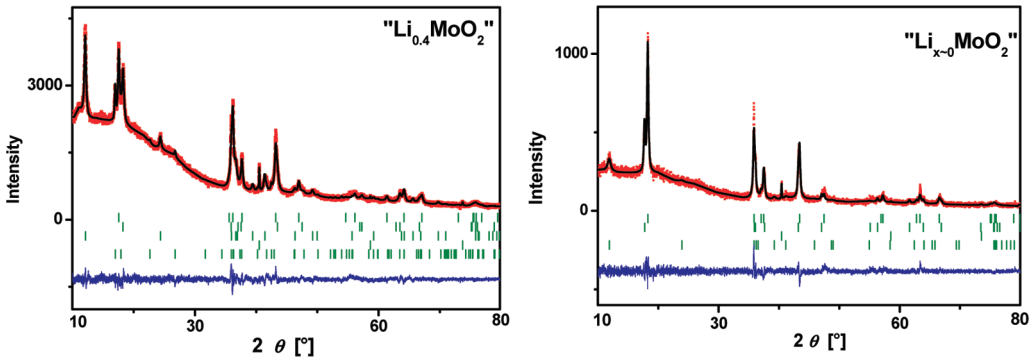

Figure 12. Measured (Cu Kα_1 radiation, λ = 1.54059 Å) and calculated powder diffraction patterns for $Li_{0.4}MoO_2$ (left) and $Li_{x\approx0}MoO_2$ (right) obtained in electrochemical test cells.Tick marks correspond to the following phases: two rhombohedral modifications (*R*-3*m*) with different lattice parameters, $(MoO_2)(PF_6)_x$, metallic Mo and monoclinic phase (*C*2/*m*) for $Li_{0.4}MoO_2$; and two rhombohedral forms, metallic Mo and $(MoO_2)(PF_6)_x$ for $Li_{x\approx0}MoO_2$.

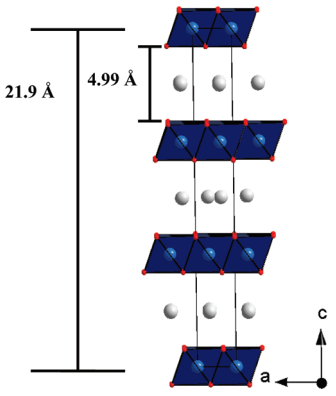

Figure 13. Crystal structure of $(MoO_2)(PF_6)_x$ with a random distribution of PF_6 (light gray spheres) between layers.

rhombohedral forms for $x = 0$ (Figure 12). Additionally, reflections of another phase with the first one corresponding to *d*-values of 7.3−7.4 Å were observed in the diffraction patterns of strongly oxidized materials together with some increased amount of metallic molybdenum in comparison to the pristine material. A disproportionation of molybdenum in $Li_{x\approx0}MoO_2$ into Mo(0) and Mo^{4+x} together with oxidation could be proposed.

A rhombohedral unit cell with much longer *c*-parameter of ~21 Å could explain observed reflections at small 2θ angles, leading to a much longer distance between Mo−O layers than expected for interlayer Li atoms. In situ synchrotron data showed that Li extraction from the rhombohedral modification is accompanied with a decreasing of the lattice parameter *c* because the oxidation of Mo reduces the negative charge of Mo−O layers, so that a huge space between neighbored Mo layers can be occupied by large cations or molecules for structure stabilization. For example, Tarascon[1] described water-containing phases $Li_{1.33}(H_2O)_{0.95}Mo_2O_4$ and $Li_2(H_2O)_{0.75}Mo_2O_4$ with larger distances between MoO_2 layers, obtained in contact with water. Insertion of a large cation can take place at much lower potentials reducing the average oxidation state of Mo. At high voltages, only Mo oxidation or disproportion could occur. The oxidation of molybdenum in MoO_2 layers leads to their positive charging and, therefore, an appearance of strong repulsive forces between them. Insertion of anions such as PF_6^- from the $LiPF_6$-containing electrolyte could take place if the average oxidation state of Mo becomes higher than +4 because Mo−O layers get positively charged. According to the work,[23] PF_6^- anion in $LiPF_6$ represents a regular octahedron with the P−F bond length of 1.60 Å and can be considered as a sphere with a diameter of about 3.2 Å. Electrochemical intercalation of PF_6 groups into the graphite structure at voltages above 5 V was investigated by Seel and Dahn[24] and gives a series of staged phases.

A crystal structure model of layered K_xNiO_2 (potassium nickelate II) with randomly distributed K^+ ions between NiO_2 layers[25] was successfully applied for structure refinement of the unknown rhombohedral phase. The resulting structure represents a sequence of MoO_6 octahedra and oxygen trigonal prisms (Figure 13), which can be statistically occupied by large atoms or atom groups. In the case of potassium nickel oxide, K_xNiO_2, K^+ ions and water molecules occupy these prisms. The value of the *c*-parameter is directly dependent on their amount. In the case of oxidized $Li_{x\approx0}MoO_2$, anions such as PF_6^- can be intercalated between MoO_2 layers and hold them together electrostatically through the compensation of their positive charge. The refinement of such a $(MoO_2)(PF_6)_x$ structure model gave the parameters listed in Table 3. Accordingly, about 4% of all trigonal prisms are occupied by PF_6 anions. The average oxygen−oxygen interatomic distance between MoO_2 layers is about 4.9941(2) Å. Different electronic states of P, F and Mo for the sample obtained at 4.5−5 V in comparison with the phases existing at lower voltage were detected by XPS investigations, see Chapter 5, and confirm indirectly the proposed intercalated model.

4.2. Chemical Oxidation of $Li_{1.0}MoO_2$. Using strong oxidizing agents such as NO_2PF_6 or NO_2BF_4 with the oxidation potential against the Li^+/Li pair of about 5 V leads to more nonequilibrium conditions and, therefore, the synthesis products should depend strongly on the reaction time. Actually, after the reaction of NO_2BF_4 or NO_2PF_6 with pristine $Li_{1.0}MoO_2$ material (1:1 molar ratio) after one day, the disappearance of the monoclinic form and a formation of the second rhombohedral phase was observed with a slightly shorter *c*-parameter (about 1% difference compared to the pristine phase) similar to the one formed during electrochemical Li extraction from Li_xMoO_2 for $x \leq 0.35$. The molybdenum content in the sample has not changed. This sample was further investigated with respect to its thermal stability (see below).

After reaction time of one week, quite different products were observed, namely a significant amount of metallic Mo, rhombohedral Li_xMoO_2 with lattice parameters slightly different from

dx.doi.org/10.1021/cm2010715 |*Chem. Mater.* 2011, 23, 3429–3441

Table 3. Structure Parameters for the Rhombohedral $(MoO_2)(PF_6)_x$ Phase, Refined on the Basis of X-ray Powder Diffraction Data[a]

$(MoO_2)(PF_6)_{0.04}$, *R*-3*m*, *a* = 2.8997(2) Å, *c* = 21.933(3) Å, *Z* = 3, *V* = 159.71(3) Å^3							
Bragg R-factor 4.88, R_f-factor 6.68							
atom	site	*x*	*y*	*z*	occup.	*d*(Mo−O), Å	d(O−O), Å
Mo	3*a*	0	0	0	1		
(PF_6)	6*c*	0	0	0.180(3)	0.043(1)	2.0358(1)	2.8584(2)
O	6*c*	0	0	0.3862(1)	1		

[a] The relevant shortest interatomic distances (in Å) are also given.

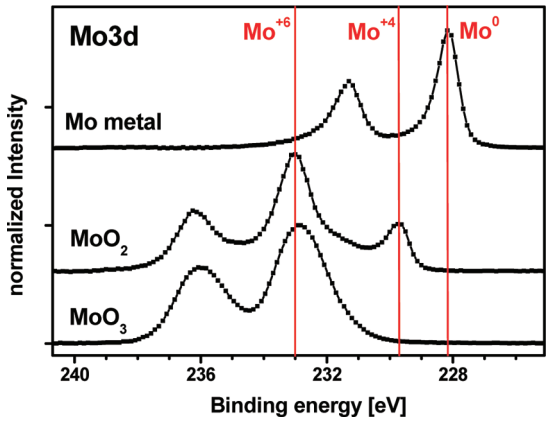

Figure 14. Mo3d spectra from reference standards metallic Mo, MoO_2, and MoO_3 (from top to bottom). The MoO_2 spectrum contains molybdenum in two oxidation states +4 and +6 due to surface oxidation. $Mo3d_{5/2}$ peaks for Mo(0), Mo(+4), and Mo(+6) correspond to 228.2, 229.8, and 233.0 eV, respectively.

the pristine rhombohedral Li_xMoO_2, rhombohedral phase with a much longer *c*-parameter of ~21 Å, cubic Li_4MoO_5, and rhombohedral Li_2MoO_4 with Mo(VI) (XRD pattern is not shown). A formation of the rhombohedral phase with much larger *c*-parameter was observed after reaction with NO_2PF_6 and NO_2BF_4 oxidizing agents. BF_4^- molecules form regular tetrahedra with a B−F bond length of 1.39 Å, which can connect MoO_2 layers together similar to PF_6 molecules. Thus, a disproportionation of Mo(4+) into Mo(0) and Mo in oxidation states higher than +4 together with a formation of $(MoO_2)(BF_4)_x$ or $(MoO_2)(PF_6)_x$ phase took place after a long reaction time.

5. XPS Studies of Electrochemically Oxidized Li_xMoO_2 Phases. Electrochemically oxidized samples were investigated by a quasi in situ XPS method[19] using the transfer of the samples, charged to different voltages and immediately disassembled in the glove box, with a transport chamber from the glove box to the XPS chamber. All the spectra are normalized for better comparison in intensity and corrected in binding energy by using the photoemission line of carbon (C1s) at 284.8 eV. In order to distinguish 3d peak positions of Mo as a function of its oxidation state, sputtered Mo powder, MoO_2, and MoO_3 were tested first as reference standards (Figure 14). In oxide materials, Mo has an octahedral surrounding of oxygen atoms. Test measurements showed $Mo3d_{5/2}$ peaks for Mo(0), Mo(+4), and Mo(+6) corresponding to 228.2, 229.8, and 233.0 eV, respectively.[26] These $Mo3d_{5/2}$ peak positions are marked in Figure 14 by vertical lines. Note that for each of these peaks a corresponding $Mo3d_{3/2}$ peak is found at 3.1 eV higher binding energy.

Mo3d spectra of the pristine $Li_{1.0}MoO_2$ and of the material charged up to 3.35 V, which corresponds to the composition $Li_{0.6}MoO_2$ calculated from the current flowed in the electrochemical test cell, are very similar to the one of MoO_2, demonstrating the presence of Mo in the mixed oxidation states +4 and +6 (Figure 15). The F1s spectra of $Li_{1.0}MoO_2$ and $Li_{0.6}MoO_2$ are also very similar (Figure 15). Two main F1s peaks around 686 and 688 eV were observed, originating from surface Li fluoride and from the PVDF binder material typically found in cathode mixtures.[20] Material with the composition $Li_{0.4}MoO_2$, charged up to 4.4 V, tends to have additional electronic states of Mo and F (marked by dotted vertical line). Mo3d spectrum showed peaks of Mo(+6) and a $Mo3d_{5/2}$ peak at 231.0 eV, corresponding to a quite different electronic state of Mo (Figure 15). The F1s spectrum of $Li_{0.4}MoO_2$ material exhibits also an additional peak at 688.8 eV, which is not present in the spectra of pristine $Li_{1.0}MoO_2$ and $Li_{0.6}MoO_2$ material. The observed additional electronic states of Mo and F for the material, electrochemically charged up to 4.4 V, could reflect the proposed $(MoO_2)(PF_6)_x$ phase formation at high voltage, accompanied by the additional reflections at 7.3−7.4 Å in the X-ray diffraction patterns (Figure 12). To prove it, quasi in situ XPS measurements were performed on $Li_{1.0}MoO_2$, cycled 30 times between 3.0 and 4.5 V, and $Li_{1.0}MoO_2$, electrochemically delithiated in the first cycle to $Li_{x=0}MoO_2$, in cells with electrolyte containing either $LiPF_6$ or LiBOB conducting salts (Figure 16). Mo3d spectra of $Li_{x=0}MoO_2$ and $Li_{1.0}MoO_2$ after 30 cycles using $LiPF_6$ are similar to the one of $Li_{0.4}MoO_2$ and showed an intensive $Mo3d_{5/2}$ peak at 231.0 eV (dotted line) together with Mo3d peaks corresponding to Mo(+6), while the Mo3d spectrum of $Li_{1.0}MoO_2$ after 30 cycles using LiBOB demonstrated only the presence of Mo(+6), and the Mo3d spectrum of $Li_{x=0}MoO_2$ after LiBOB a Mo(+6)-like state. F1s spectra of $Li_{x=0}MoO_2$ and $Li_{1.0}MoO_2$ after 30 cycles using $LiPF_6$ exhibit a very intensive peak around 689 eV (dotted line), which does not exist in the F1s spectra of pristine $Li_{1.0}MoO_2$ and $Li_{0.6}MoO_2$. This observation is in agreement with the proposal of a further oxidation of Mo and a $(MoO_2)(PF_6)_x$ formation at voltages above 4.0 V. Note that the $(MoO_2)(PF_6)_x$ phase does not disappear completely, at least not from the surface, after cycling and partial electrochemical reduction by decreasing the voltage again to 3.0 V; the high level of oxidation of Mo is at least not completely reversible.

6. High-Temperature Structural Investigations of Lithium-Poor Li_xMoO_2 ($x \approx 0$). A metastable character of Li-deficient phases against heating with successive phase transformations at elevated temperatures can be expected for Li_xMoO_2, similar to Li_xCoO_2.[9] In contrast to compounds with 3d transition metals,

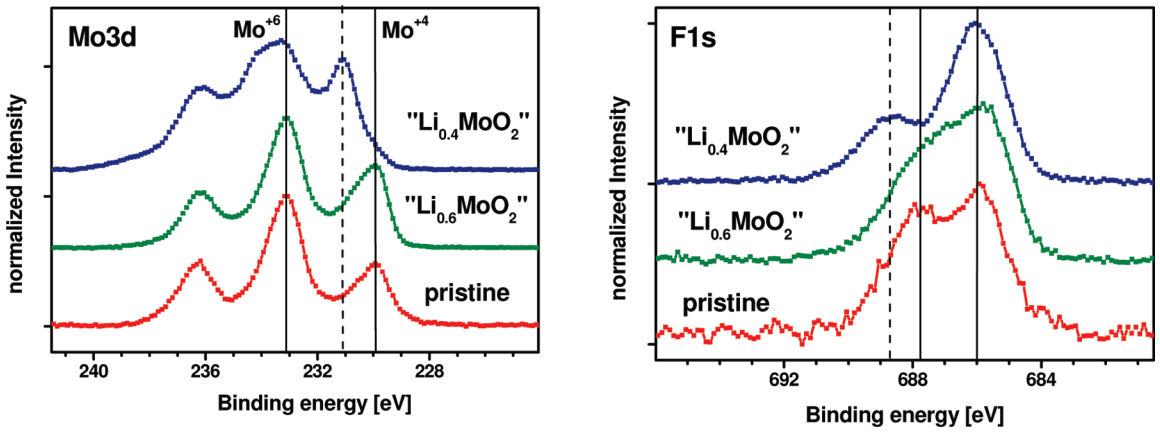

Figure 15. Mo3d and F1s spectra of the pristine cathode mixture $LiMoO_2$, electrochemically delithiated $Li_{0.6}MoO_2$ at the upper volatge limit voltage of 3.35 V, and $Li_{0.4}MoO_2$ at 4.4 V. $LiPF_6$ was used as the conducting salt in the electrolyte.

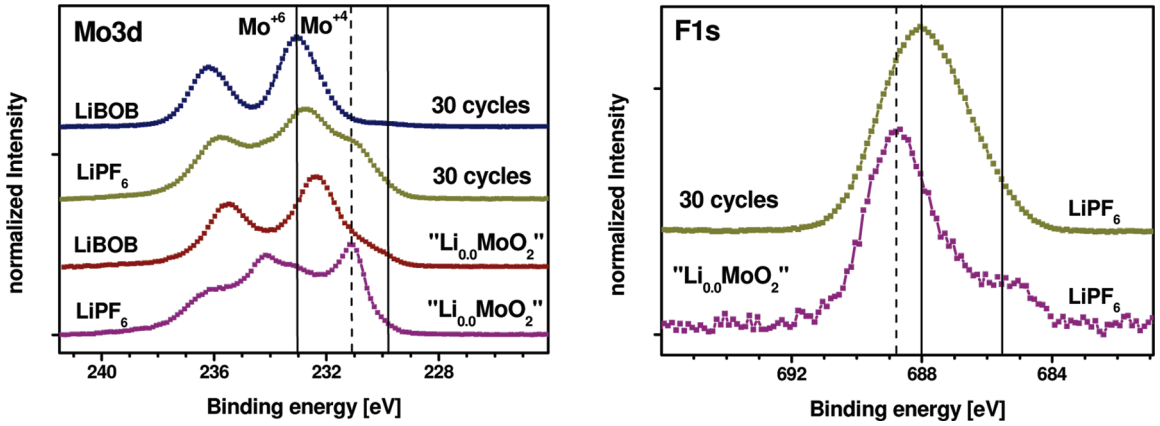

Figure 16. Mo3d and F1s spectra of $LiMoO_2$, electrochemically delithiated to $Li_{x\approx 0.0}MoO_2$, and $LiMoO_2$ cycled 30 times between 3.5 and 4.0 V using $LiPF_6$ and LiBOB as electrolyte salts. F1s spectra after using LiBOB showed only weak peak at about 686 eV. $Li_{x\approx 0.0}MoO_2$ with LiBOB was obtained at 4.8 V and at about 5.1 V using $LiPF_6$ in the electrolyte.

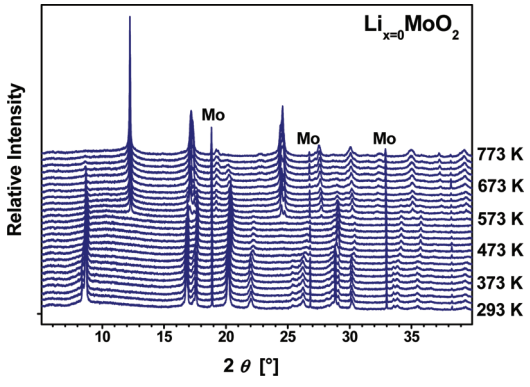

Figure 17. In situ thermal stability investigations in Ar by synchrotron diffraction on $Li_{x\approx 0}MoO_2$, obtained by the chemical route. An irreversible phase transformation takes place at about 573 K.

Mo(IV)-containing oxides hardly release any oxygen, which would be accompanied by a decrease in the average oxidation state of the transition metal. A disproportion of molybdenum could be expected instead. The $Li_{x\approx 0}MoO_2$ sample contains two layered rhombohedral modifications, Li_xMoO_2 (R-3m) with x-values close to 0 and metallic Mo and undergoes a phase transition at 573 K into a monoclinic "Li_xMoO_2" form, isostructural to MoO_2 ($P2_1/c$)[27] with lattice parameters a = 5.6650(1) Å, b = 4.8671(1) Å, c = 5.6476(1) Å, β = 120.849(1)° at 773 K and a mixed occupancy of the 4e site by Li (15%) and Mo (85%) (Figure 17). The formed phase belongs to the rutile structure type with a three-dimensional network (Figure 18) and remains stable after cooling to room temperature. The shortest interatomic Mo−Mo distance of 2.59 Å indicates metallic Mo−Mo bonds within Mo_2O_{10} clusters (Figure 19).

DISCUSSION

$Li_x(Mo_{1-y}Li_y)O_2$ compounds possess several structural and chemical degrees of freedom, like Li content, which is coupled with the average oxidation state of molybdenum, space group symmetry, mixed occupancy of cation sites by Li and Mo, and metallic Mo−Mo bond formation into either clusters or endless chains. Because of the high intralayer Li diffusion, all these parameters are severely temperature dependent. The structure investigations of a mixture of rhombohedral and monoclinic phases with $Li_{1.0}MoO_2$ composition during heating in inert atmosphere

dx.doi.org/10.1021/cm2010715 |Chem. Mater. 2011, 23, 3429–3441

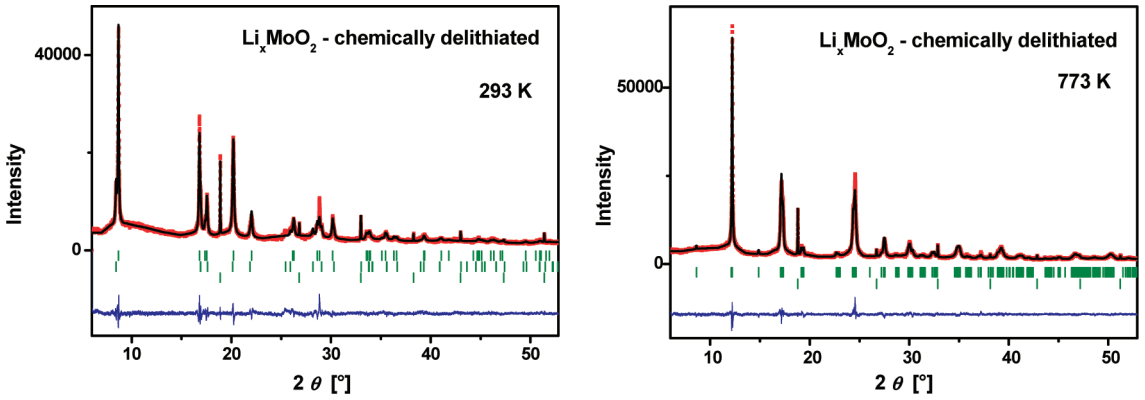

Figure 18. Synchrotron diffraction patterns together with calculated and difference curves. Left: Pristine $Li_{x\approx0}MoO_2$ material containing two rhombohedral modifications and metallic Mo. Right: $Li_{x\approx0}MoO_2$ after the phase transformation at 773 K. The monoclinic MoO_2 phase ($P2_1/c$) was used as the structure model for the refinement.

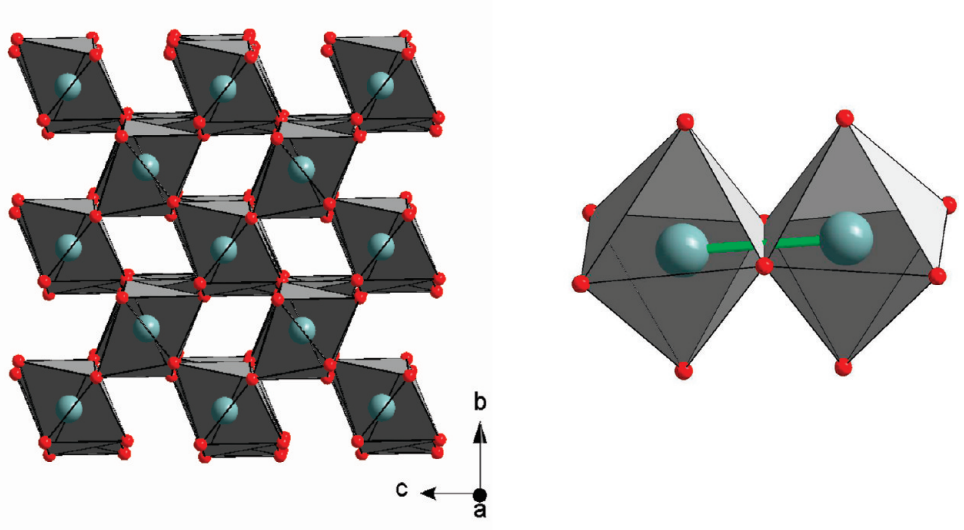

Figure 19. Crystal structure of monoclinic rutile-type $(Mo,Li)O_2$ (left) with Mo_2O_{10} clusters (right).

reflected a redistribution of Mo, accompanied by Li_2MoO_4 formation, already at 423 K. It confirms a high Li mobility even at moderate temperatures and a very complicated temperature-dependent phase relationship in the Li−Mo−O system.

During electrochemical Li extraction and insertion from or into an initial $Li_{1.0}MoO_2$ cathode, containing the monoclinic and rhombohedral Li_xMoO_2 phases, the monoclinic one becomes unstable under Li extraction and decomposes into two rhombohedral phases: one with lattice parameters similar to the pristine form and another one with shorter *c*-parameters, which suggests nearly a Li-free composition $Li_{x\approx0}MoO_2$. This Li-poor phase is sensitive against further oxidation and can be "irreversibly" stabilized via intercalation of large anions such as PF_6^- or $BF4^-$ between MoO_2 layers. Note that high-temperature synthesis and Li deficiency support the formation of phases with monoclinic symmetry and metallic Mo−Mo bonds, while delithiation at room temperature favors the rhombohedral form without metallic bonds. This nearly Li-free rhombohedral form transforms into a rutile-type network structure with metallic Mo−Mo bonds at elevated temperature (573 K).

The rhombohedral Li_xMoO_2 modification appears to be a more suitable electrode material in comparison to the monoclinic form because of the instability of monoclinic Li_xMoO_2 against Li extraction. Electrochemical studies on rhombohedral Li_2MoO_3[28] revealed a promising electrode material with the first discharge capacity of about 200 mAh/g. On the one hand, James et al[7] reported about a non-topotactical one-phase mechanism of Li deinsertion from rhombohedral Li_2MoO_3, accompanied by an irreversible moving of Mo from "Mo" layers into "Li" layers with hindering Li diffusion and, therefore, leads to a worse kinetic of electrochemical lithiation/delithiation in such a cathode material. The non-monotonous decrease of the c/a ratio during Li extraction from Li_2MoO_3, reported in refs 7, 29, should support this model. On the other hand, this non-monotonous decrease of the c/a ratio could result from repulsion between oxygen atoms in neighboring layers and the shortening of Mo−O distances from an increase of the average oxidation state of Mo.

Synchrotron diffraction during electrochemical Li extraction reported in the present work did not detect any redistribution of Mo atoms in the rhombohedral form with a slight Li excess over $Mo,Li_x(Mo_{1-y}Li_y)O_2$. In contrast, such a redistribution of Mo is reported in the literature for Li_2MoO_3 with a high degree of mixed occupation of the cation site(s) by Li and Mo. Such a

dx.doi.org/10.1021/cm2010715 |*Chem. Mater.* 2011, 23, 3429–3441

mixed occupation probably provides sufficient lattice defects (cation vacancies) during delithiation, which facilitate a high Mo mobility and lead to an irreversible Mo transport onto Li layers. Therefore, rhombohedral phases with a slight Li excess seem to be the most promising candidates for an application as cathode material in lithium ion batteries.

CONCLUSION

Different crystal structures of Li_xMoO_2 were analyzed by single crystal X-ray diffraction. The composition $Li_{1.0}MoO_2$ synthesized by solid-state reaction at high temperature represents a mixture of the rhombohedral form without metallic Mo−Mo bonding and the monoclinic form with endless zigzag metallic Mo chains. Detailed in situ structural investigations of $Li_{1.0}MoO_2$ cathode material during Li extraction and insertion revealed at low Li contents a reversible transformation of the monoclinic form into two rhombohedral modifications with different Li contents, while the pristine rhombohedral form demonstrates topotactical Li extraction and insertion.

AUTHOR INFORMATION

Corresponding Author

*E-mail: d.mikhailova@ifw-dresden.de.

ACKNOWLEDGMENT

This work was supported by the DFG Research Collaborative Centre 595 "Electrical Fatigue in Functional Materials" and by the Federal Ministry of Education and Research (BMBF). The authors are thankful to A. Voss for performing the chemical analyses by ICP-OES.

REFERENCES

(1) Tarascon, J. M. *J. Electrochem. Soc.* **1987**, *134*, 1345–1351.
(2) Barker, J.; Saidi, M. Y.; Swoyer, J. L. *Electrochem. Solid-State Lett.* **2003**, *6*, A252–256.
(3) Colson, S.; Szu, S.-P.; Klein, L. C.; Tarascon, J. M. *Solid State Ionics* **1991**, *46*, 283–289.
(4) Aleandri, L. E.; McCarley, R. E. *Inorg. Chem.* **1988**, *27*, 1041–1044.
(5) Hibble, S. J.; Fawcett, I. D.; Hannon, A. C. *Inorg. Chem.* **1997**, *36*, 1749–1753.
(6) Takahaski, Y.; Kijima, N.; Hayakawa, H.; Awaka, J.; Akimoto, J. *J. Phys. Chem. Sol* **2008**, *69*, 1518–1520.
(7) James, A. C. W. P.; Goodenough, J. B. *J. Solid State Chem.* **1988**, *76*, 87–96.
(8) Reau, J.-M.; Fouassier, C.; Hagenmuller, P. *J. Solid State Chem.* **1970**, *1*, 326.
(9) Dahn, J. R.; Fuller, E. W.; Obrovac, M.; von Sacken, U. *Solid State Ionics* **1994**, *69*, 265–270.
(10) Cox, D. E.; Cava, R. J.; McWhan, D. B.; Murphy, D. W. *J. Phys. Chem. Sol.* **1982**, *43*, 657–666.
(11) Sheldrick, G. M. *Acta Crystallogr.* **1990**, *A46*, 467–473.
(12) Sheldrick, G. M. *SHELXL97, Program for the Refinement of Crystal Structures*; University of Göttingen: Germany, 1997.
(13) *X-STEP32*; Stoe & Cie GmbH: Darmstadt, Germany, 2000.
(14) *CrysalisRed, CCD Data Reduction GUI*, version 1.171.26; Oxford Diffraction: Poland, 2005.
(15) Hoelzel, M.; Senyshyn, A.; Gilles, R.; Boysen, H.; Fuess, H. *Neutron News* **2008**, *18*, 23.
(16) Knapp, M.; Baehtz, C.; Ehrenberg, H.; Fuess, H. *J. Synchrotron Rad.* **2004**, *11*, 328–334.
(17) Knapp, M.; Joco, V.; Baehtz, C.; Brecht, H. H.; Berghaeuser, A.; Ehrenberg, H.; von Seggern, H.; Fuess, H. *Nucl. Instrum. Meth.* **2004**, *A 521*, 565–570.
(18) Baehtz, C.; Buhrmester, T.; Bramnik, N. N.; Nikolowski, K.; Ehrenberg, H. *Solid State Ionics* **2005**, *176*, 1647–1652.
(19) Nikolowski, K.; Baehtz, C.; Bramnik, N. N.; Ehrenberg, H. *J. Appl. Crystallogr.* **2005**, *38*, 851–853.
(20) Oswald, S.; Nikolowski, K.; Ehrenberg, H. *Anal. Bioanal. Chem.* **2009**, *393*, 1871–1877.
(21) *Inorganic Crystal Structure Database (ICSD)*; Fachinformationszentrum: Karlsruhe, Germany, 2010−2011.
(22) Laubach, So.; Laubach, S.; Schmidt, P. C.; Ensling, D.; Schmid, S.; Jaegermann, W.; Thissen, A.; Nikolowski, K.; Ehrenberg, H. *Phys. Chem. Chem. Phys.* **2009**, *11*, 3278–3289.
(23) Rohr, C.; Kniep, R. *Z. Naturforsch.* **1994**, *49*, 650–654.
(24) Seel, J. A.; Dahn, J. R. *J. Electrochem. Soc.* **2000**, *147*, 892–898.
(25) Bityntskii, P. N.; Khitrova, V. I. *Kristallografiya* **1969**, *14*, 122–126.
(26) Choi, J.-G.; Thompson, L. T. *Appl. Surf. Sci.* **1996**, *93*, 143–149.
(27) Brandt, B. G.; Skapski, A. C. *Acta Chem. Scand.* **1967**, *21*, 661–672.
(28) Kobayashi, H.; Tabuchi, M.; Shikano, M.; Nishimura, Y.; Kageyama, H.; Ishida, T.; Nakamura, H.; Kurioka, Y.; Kanno, R. *J. Power Sources* **1999**, *81−82*, 524–529.
(29) Gopalakrishnan, J.; Bhat, V. *Mater. Res. Bull.* **1987**, *22*, 769–774.